The Journal of Chemical Physics

Molecular rotation in 3 dimensions at an air/water interface using femtosecond time resolved sum frequency generation

Cite as: J. Chem. Phys. **150**, 094709 (2019); https://doi.org/10.1063/1.5080228@jcp.2019.NSISD.issue-1
Submitted: 06 November 2018 . Accepted: 15 February 2019 . Published Online: 07 March 2019

Yi Rao, Yuqin Qian, Gang-Hua Deng, Ashlie Kinross, Nicholas J. Turro, and Kenneth B. Eisenthal

COLLECTIONS

Paper published as part of the special topic on Collection and Nonlinear Spectroscopy and Interfacial Structure and Dynamics
Note: This article is part of the Special Topic "Nonlinear Spectroscopy and Interfacial Structure and Dynamics" in J. Chem. Phys.

View Online Export Citation CrossMark

ARTICLES YOU MAY BE INTERESTED IN

Development of ultrafast broadband electronic sum frequency generation for charge dynamics at surfaces and interfaces
The Journal of Chemical Physics **150**, 024708 (2019); https://doi.org/10.1063/1.5063458

Water structure at the interface of alcohol monolayers as determined by molecular dynamics simulations and computational vibrational sum-frequency generation spectroscopy
The Journal of Chemical Physics **150**, 034701 (2019); https://doi.org/10.1063/1.5072754

Heterodyne transient vibrational SFG to reveal molecular responses to interfacial charge transfer
The Journal of Chemical Physics **150**, 114706 (2019); https://doi.org/10.1063/1.5066237

© 2019 Author(s).

The Journal of Chemical Physics ARTICLE scitation.org/journal/jcp

Molecular rotation in 3 dimensions at an air/water interface using femtosecond time resolved sum frequency generation

Cite as: J. Chem. Phys. 150, 094709 (2019); doi: 10.1063/1.5080228
Submitted: 6 November 2018 • Accepted: 15 February 2019 •
Published Online: 7 March 2019

View Online Export Citation CrossMark

Yi Rao,[1,a)] Yuqin Qian,[1] Gang-Hua Deng,[1] Ashlie Kinross,[1] Nicholas J. Turro,[2] and Kenneth B. Eisenthal[2,a)]

AFFILIATIONS

[1] Department of Chemistry and Biochemistry, Utah State University, Logan, Utah 84322, USA
[2] Department of Chemistry, Columbia University, New York, New York 10025, USA

Note: This article is part of the Special Topic "Nonlinear Spectroscopy and Interfacial Structure and Dynamics" in J. Chem. Phys.
[a)] **Authors to whom correspondence should be addressed:** yi.rao@usu.edu and kbe1@columbia.edu.

ABSTRACT

This paper presents the first study of the rotations of rigid molecules in 3 dimensions at the air/water interface, using the femtosecond time resolved sum frequency generation (SFG) technique. For the purpose of this research, the aromatic dye molecule C153 was chosen as an example of a molecule having two functional groups that are SFG active, one being the hydrophilic −C=O group and the other the hydrophobic $-CF_3$ group. From polarized SFG measurements, the orientations of the two chromophores with respect to the surface normal were obtained. On combining these results with the known relative orientation of the two chromophores in the molecule yields the absolute orientation of C153 at the air/water interface. It was found that the $-CF_3$ axis projected towards the bulk air at an angle of 59° with respect to the interface normal and the −C=O group projected towards the bulk water at an angle of 144°. In order to observe the rotational motions of C153 at the air/water interface, the approach was used to perturb the ground electronic state equilibrium orientational distribution using a polarized resonant pump pulse, which preferentially excites ground state molecules that have their electronic $S_0 \rightarrow S_1$ transition moment aligned closely to the electric field of the incident pump pulse. As a consequence of the photoselection perturbation, the orientational distribution of the remaining ground state molecules was not the equilibrium distribution. Similarly, the orientational distribution of the excited state molecules that were created by the polarized pump pulse was not in their final equilibrium orientational distribution. The rotational motions of the interfacial molecules towards equilibrium were obtained from time dependent measurements of the intensities of the SFG signal generated by the simultaneous incidence at the air/water interface of a visible probe pulse plus an IR probe pulse. In this way, the recovery times to achieve the orientational equilibrium of the two chromophores including the orientation of the normal of the C153 plane with respect to the interface were obtained. The photo-selection process shifts the average orientation angle of the hydrophilic −C=O group by an increase of 4° ± 0.6° with a rotational recovery time constant of 130 ± 20 ps, which is the time to return to an orientational equilibrium distribution. The hydrophobic $-CF_3$ group undergoes a shift that increases its angle by 8° ± 1.5° with a rotational recovery time constant of 210 ± 38 ps. We find that the orientational change of the molecular normal is 4° ± 0.5° and has a rotational recovery time constant of 125 ± 26 ps. The interface-specific time-dependent polarized measurements allowed us to monitor the orientational motions of molecules at interfaces, both in 3 dimensions and in real time.

Published under license by AIP Publishing. https://doi.org/10.1063/1.5080228

I. INTRODUCTION

Interfaces are the molecularly thin regions of matter which separate distinct physical and/or chemical bulk regions of matter. Intrinsic anisotropic geometry of interfaces is the origin of their unique chemical, physical, and biological properties. Water interfaces are predominant on our planet, of which the air/water interface is the most important in covering more than 2/3 of the Earth's surface. Of note are the mineral oxide/water interfaces as that is an important location where soil chemistry chiefly takes place. Of

Published under license by AIP Publishing

special significance are biological cell membrane/water interfaces as they are central to life processes.

Interfaces not only have different properties from the regions that bound them but also serve as the gate keeper that controls the passage of all energy, radiation, and chemical species between the adjacent phases. The lower symmetry of the interface plays a key role in determining the orientational structure, chemical composition, chemical and physical equilibria, and other time independent properties as well as time dependent molecular motions, chemical transformations, energy and charge transfer, and others.

Second Harmonic Generation (SHG) is a second order optical process that depends primarily on the electronic properties of the interfacial molecules, while Sum Frequency Generation (SFG) is another second order optical process which is sensitive to molecular vibrations when one incident beam is tuned in the infrared region that corresponds to an interfacial SFG allowed vibration. Both processes can be employed to specifically investigate interfaces that are accessible to light, including buried interfaces.[1–4] Static SHG and SFG measurements provide valuable information about the populations of interfacial species, molecular orientational ordering, acid-base equilibrium, etc., occurring at an interface.[5–24] Time-resolved SHG has also been used to study solvation dynamics, rotational dynamics, electron transfer, population recovery, two-dimensional energy transfer, and other ultra-fast processes.[25–30] SFG is a powerful method to investigate structural dynamics, vibrational energy relaxation, thermal transport, and other interfacial processes.[19,31–37] In recent work, we have used visible-pump-time-resolved vibrational SFG experiments to study rotational dynamics of a single chemical group of a molecule at the air/water interface using the visible-pump-SFG probe technique.[32] In the work reported here, we exploit this technique to observe the rotational dynamics of a molecule in 3 dimensions by measuring the rotational dynamics of two chromophores of a selected molecule which are not collinearly oriented on the molecule.

Molecules assume orientations that lower the free energy in the interfacial region. At the air/water interface, this orientation generally will align a polar non-hydrogen bonding adsorbate with its more polar part projecting into the water phase and the less polar part towards the air. After excitation, molecular motions occur returning the adsorbates back to the lower free energy orientation. The orientations and rotational motions of interfacial molecules can be utilized as sensitive probes of the unique asymmetric environment that interfacial chemical species experience. For hydrogen bonding adsorbates such as phenol, we have found from absolute phase measurements that the hydroxyl group points down (towards the water), which is also the direction of the permanent dipole moment of phenol. Unlike phenol both nitrophenol and bromophenol have their permanent dipole moments in the opposite direction to that of phenol. The question is then "Is it the permanent dipole moment or is it the hydrogen bonding hydroxyl group that determines the up towards the air vs down towards the water orientation?" Phase measurements in our lab showed that phenol, bromophenol, and nitrophenol all have their hydroxyl group pointing towards the bulk water.[38] This displays the hydrogen bonding dominance. It is the hydrogen bonding of the hydroxyl group with water rather than the dipole moment direction that determines the up-down alignment of these molecules at the air/water interface.

The in-plane orientational distribution of adsorbates at the air/water interface is, on average, isotropic because the in-plane intermolecular forces are, on average, isotropic in the interfacial plane. The intermolecular forces that are out-of-plane with respect to the interface, i.e., the air above and water below, are anisotropic. This anisotropy is responsible for the adsorbate orientation, given by the polar angle θ. Just as the equilibrium orientational distribution in θ is restricted by the asymmetry of the interfacial potential, the translational and rotational motions of interfacial molecules are restricted by the asymmetric potential of the interface. Unlike the bulk water, in which rotational motions occur in all directions with equal probability, the dynamics of rotation in the interfacial plane differ from rotations out of the interfacial plane. In earlier SHG studies of orientational relaxation, the rotation dynamics of a single symmetry axis about the interfacial normal[29,30,39–41] was obtained. In the work reported here, the objective was to measure the interfacial rotation dynamics of the whole molecule, i.e., rotation of the molecule in three dimensions. Employing a procedure used in earlier work,[42] we obtained the absolute orientation of the interfacial molecule. This was accomplished by measuring the orientations with respect to the surface normal of two SFG active vibrational chromophores that are not collinear in a rigid molecule. Furthermore, it was assumed that the up vs. down alignment of the molecule in the interface is known. It was assumed that the orientational distribution is given by a delta function. This will be briefly discussed at a later point.

Experiments using time-resolved sum frequency measurements were used to obtain the absolute orientation of two chromophores as the molecules rotate toward their equilibrium orientations. Time-resolved polarized SFG experiments used a pump pulse to photoselect an orientational subset of the equilibrium distribution of ground state molecules, which thereby generate a non-equilibrium orientational distribution in both the ground state molecules that were not excited and the excited state molecules produced by the pump pulse.[27,28,30,32,39,40] Depending on the polarization of the pump pulse, the change in the SFG intensity with time can depend on both in-plane and out-of-plane rotations. It has been shown that the out-of-plane rotations can be separated from the in-plane rotations by using a circularly polarized laser pump pulse that is incident normal to the interfacial plane.[40] At a resonant pump frequency, the interfacial molecules were excited to their lowest excited singlet state. The ground state molecules, prior to the pump pulse, were isotropically distributed in the interfacial plane because of the inherent in-plane isotropy of forces at the air/water interface. The circularly polarized pump light has the same intensity in all directions parallel to the interface plane. Both the remaining ground and excited state molecules were at all times isotropically distributed in the interface plane. The in-plane distribution of molecules, therefore, has no time-dependent change because these molecules are always isotropic in the plane of the interface. However, because the pump light preferentially excites molecules whose transition moments are parallel to the polarization of the pump electric field, the out-of-plane orientational distribution of the ground state molecules that were and were not excited is not in their equilibrium orientational distributions. It is the evolution of the out-of-plane orientational distribution from nonequilibrium to equilibrium that is achieved by rotational motions of the interfacial molecules

Published under license by AIP Publishing

that we observed. To study the in-plane rotational dynamics, the first step is to break the initial isotropic symmetry of the in-plane orientational distribution. This was achieved by using a linearly polarized pump light, e.g., along the in-plane X-axis, which photoinduces an in-plane orientational anisotropy (fewer unexcited ground state molecules oriented along the X-axis). In the work reported here, we will mainly focus on the out-of-plane motion of molecules at the air/water interface.

II. THEORETICAL CONSIDERATIONS

A. Static SFG and interfacial order parameter D ($-\infty$) at equilibrium

The SFG intensity of any of the polarization combinations at equilibrium, I^{SFG}, is related to the surface second order susceptibility $\chi^{(2)}$. The susceptibility is the sum over all macroscopic sum frequency susceptibility terms separated into a non-resonant part $\chi^{(2)}_{NR}$ and a resonant part $\chi^{(2)}_{R}$. Thus, one is able to express the SFG intensity as the following generalized expression:[3]

$$I^{SFG} \propto \left|\chi^{(2)}_{R} + \chi^{(2)}_{NR}\right|^2. \tag{1}$$

In the case of SFG experiments, a tunable or broadband IR beam, which is resonant with the chemical groups of interest, enhances the susceptibility as expressed in the following:[3]

$$\begin{aligned} \chi^{(2)} &= \chi^{(2)}_{NR} + \sum_q \chi^{(2)}_{R,q}, \\ \chi^{(2)}_{R,q} &= \frac{A_q}{\omega - \omega_q + i\Gamma_q}, \end{aligned} \tag{2}$$

where ω_q denotes the resonant frequency of the qth vibrational normal mode, and Γ_q is the dephasing rate of the vibrational state, A_q contains the product of the Raman and infrared matrix elements of the qth normal mode. The resonant second order susceptibility of interfaces, $\chi^{(2)}_R$, is related to molecular hyperpolarizability $\alpha^{(2)}_{ijk}$ by spatial transformation from a molecular coordinate frame to the laboratory coordinate frame (Fig. 1)[43]

$$\begin{aligned} \chi^{(2)}_{IJK} &= N\sum_{ijk}\langle R_{Ii}R_{Jj}R_{Kk}\rangle\alpha^{(2)}_{ijk}, \\ \alpha^{(2)}_{q,ijk} &= \frac{a_{q,ijk}}{\omega - \omega_q + i\Gamma_q}, \end{aligned} \tag{3}$$

where R_{Ii}, R_{Jj}, and R_{Kk} are the direction cosine matrices that transform the laboratory coordinate frame (I, J, K = X, Y, Z) into the molecular coordinate frame (i, j, k = x, y, z), N is the surface density of ground-state molecules at equilibrium, and $\langle\rangle$ denotes the ensemble average of the orientational distribution $\rho_g(\theta,\ t<0)$. In SHG, it is often assumed, with some justification, that the SHG hyperpolarizability $\alpha^{(2)}$ can be treated as uniaxial with only one element $\alpha^{(2)}_{zzz}$ when the SHG wavelength is strongly resonant with a transition along the molecular axis z. However, in the case of the vibrationally resonant SFG, the hyperpolarizability $\alpha^{(2)}$ of a vibrational dipole cannot be simply considered as a single element, depending upon the symmetry of the chemical groups of interest. This arises because the electronic polarizabilities of chemical bonds, which are a measure of the response of the electrons to an external field, are usually anisotropic. Of special interest are three kinds of symmetries including $C_{\infty v}$, C_{2v}, and C_{3v}, which represent a majority of functional chemical groups. For example, there are 11 nonzero microscopic hyperpolarizability elements of the C_{3v} symmetry group such as the $-CF_3$ group, three corresponding to symmetric stretching modes and eight to asymmetric stretching modes.[17,44,45] For C_{2v} symmetry groups, such as the $-CH_2$ group, there are 7 non-vanishing molecular hyperpolarizability tensor elements, three contributing to symmetric stretching modes, and four to asymmetric stretching modes. The nonzero hyperpolarizability terms for a $C_{\infty v}$ symmetry group such as $-C{=}O$, $-CN$, $-CH$, etc., are all symmetric, with $\alpha^{(2)}_{xxz} = \alpha^{(2)}_{yyz} = r^*\alpha^{(2)}_{zzz}$, where $r = \alpha^{(2)}_{xxz}/\alpha^{(2)}_{zzz}$.[44–46]

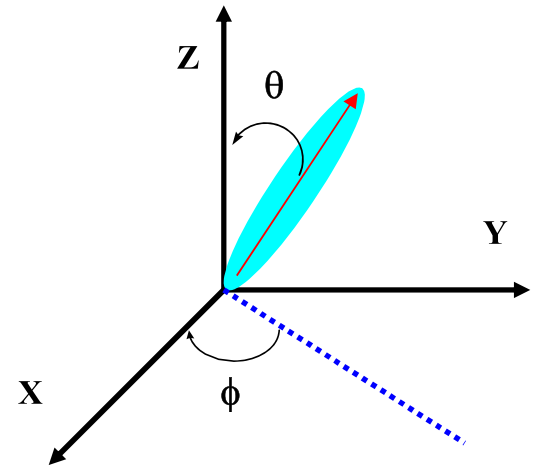

FIG. 1. A polar orientation of a dipole in the laboratory coordinate frame.

At liquid surfaces, only the seven elements $\chi^{(2)}_{XZX} = \chi^{(2)}_{YZY}$, $\chi^{(2)}_{ZXX} = \chi^{(2)}_{ZYY}$, $\chi^{(2)}_{XXZ} = \chi^{(2)}_{YYZ}$, and $\chi^{(2)}_{ZZZ}$ are nonzero (the X and Y axes are equivalent for an isotropic surface).[2] Thus, before photoexcitation, the second order susceptibilities of their symmetric stretching modes are expressed as follows:[17,43]

$$\begin{aligned} \chi^{(2)}_{XXZ}(-\infty) &= \chi^{(2)}_{YYZ}(-\infty) = \frac{1}{2}N\alpha^{(2)}_{zzz}\left[(1+r)\langle\cos\theta(-\infty)\rangle - (1-r)\left\langle\cos^3\theta(-\infty)\right\rangle\right], \\ \chi^{(2)}_{XZX}(-\infty) &= \chi^{(2)}_{YZY}(-\infty) = \chi^{(2)}_{ZYY}(-\infty) = \chi^{(2)}_{ZXX}(-\infty) = \frac{1}{2}N\alpha^{(2)}_{zzz}(1-r)\left[\langle\cos\theta(-\infty)\rangle - \left\langle\cos^3\theta(-\infty)\right\rangle\right], \\ \chi^{(2)}_{ZZZ}(-\infty) &= N\alpha^{(2)}_{zzz}\left[r\langle\cos\theta(-\infty)\rangle + (1-r)\left\langle\cos^3\theta(-\infty)\right\rangle\right]. \end{aligned} \tag{4}$$

Published under license by AIP Publishing

The four polarization combinations measured in each SFG experiment were *SSP*, *PPP*, *SPS*, and *PSS*, where the first letter denotes the polarization of the sum frequency light, the second one denotes the polarization of the 400 nm light, and the last one denotes the polarization of the IR light. These polarizations are connected with the laboratory coordinates by nonlinear Fresnel coefficients and appropriate projections. The four effective susceptibilities for SFG experiments (*SSP*, *SPS*, *PSS*, *and PPP*) are related to the above seven second order susceptibilities by local field factors L_{ii} as expressed,[17,47]

$$\begin{aligned}
\chi^{(2)}_{SSP}(-\infty) &= L_{XX}L_{XX}L_{ZZ}\sin\beta_3\chi^{(2)}_{XXZ}(-\infty),\\
\chi^{(2)}_{SPS}(-\infty) &= L_{XX}L_{ZZ}L_{XX}\sin\beta_2\chi^{(2)}_{XZX}(-\infty),\\
\chi^{(2)}_{PSS}(-\infty) &= L_{ZZ}L_{XX}L_{XX}\sin\beta_1\chi^{(2)}_{ZXX}(-\infty),\\
\chi^{(2)}_{PPP}(-\infty) &= L_{ZZ}L_{ZZ}L_{ZZ}\sin\beta_1\sin\beta_2\sin\beta_3\chi^{(2)}_{ZZZ}(-\infty) + L_{ZZ}L_{YY}L_{YY}\sin\beta_1\cos\beta_2\cos\beta_3\chi^{(2)}_{ZYY}(-\infty)\\
&\quad - L_{YY}L_{ZZ}L_{YY}\cos\beta_1\sin\beta_2\cos\beta_3\chi^{(2)}_{YZY}(-\infty) - L_{YY}L_{YY}L_{ZZ}\cos\beta_1\cos\beta_2\sin\beta_3\chi^{(2)}_{YYZ}(-\infty).
\end{aligned} \tag{5}$$

By substituting Eq. (4) into Eq. (5) and then into Eq. (1), the surface susceptibility of any polarization combinations before photoexcitation, $\chi^{(2)}_{\delta\eta\xi}(-\infty)$, can be simply formulated as the following generalized expression:[27,42,48]

$$\chi^{(2)}_{\delta\eta\xi}(-\infty) = NA_{\delta\eta\xi}(\langle\cos\theta(-\infty)\rangle - c_{\delta\eta\xi}\langle\cos^3\theta(-\infty)\rangle)\alpha^{(2)}_{zzz}, \tag{6}$$

where the parameters A and c are functions of the incident and outgoing angles and the polarization angles, and the dielectric constants of both the fundamental and second harmonic light frequencies in the bulk media and in the molecular layer.

According to Eq. (6), one can measure an interfacial order parameter D(t). At equilibrium (before photo-excitation), its value can be obtained from the ratio of any two of the four polarization SFG intensities or from null-angle measurements, yielding at $t = -\infty$,

$$D(-\infty) = \frac{\langle\cos\theta(-\infty)\rangle}{\langle\cos^3\theta(-\infty)\rangle}. \tag{7}$$

The utility of the order parameter D for a delta function orientational distribution is that the measured value of D yields the orientational angle θ.

B. Transient SFG and time-dependent interfacial order parameter *D*(t)

The time evolution of the various relaxation processes following photoexcitation includes ultrafast solvation dynamics, orientational dynamics, and population recovery, all of which are well separated in time in our experiments. The solvation dynamics, which for Coumarin 314 and Coumarin 153 are a few picoseconds in duration at the air/water interface, have been discussed previously.[31,49,50] The time evolution of the orientational dynamics is often described by the conditional probability $G(\theta_t,t;\theta_0,0)$ for the molecules that have the orientation θ_t at the time t when it had the orientation θ_0 at the initial time $t = 0$. Thus, the time evolution of the orientational population for the non-equilibrium ground state is given by, $G(\theta_t,t;\theta,0)\rho_g(\theta,-\infty)N_g(t-\infty)(1-\sigma|\mu|^2|E|^2\sin^2\theta_0)$,[30] where σ is a collection of constants associated with photo-excitation, μ is the transition dipole moment, and E is the electric field of the normal incident circularly polarized pump pulse.[30]

The susceptibility element $\chi^{(2)}_{XZX}$ for the perturbed ground state, which corresponds to the *SPS* polarization combination, is taken as an example. For the perturbed ground state, we can write the time-dependent susceptibilities as follows:[27]

$$\begin{aligned}
\chi^{(2)}_{g,XZX}(t) &= A_{XZX}\alpha^{(2)}_{g,zzz}\int d\theta_t\sin\theta_t\int d\theta_0\sin\theta_0(\cos\theta_t - c_{XZX}\cos^3\theta_t)N_g(\theta,t>0)\\
&= A_{XZX}N_g(-\infty)\alpha^{(2)}_{g,zzz}\int d\theta_t\sin\theta_t\int d\theta_0\sin\theta_0(\cos\theta_t - c_{XZX}\cos^3\theta_t)G(\theta_t,t;\theta_0,0)\rho_g(\theta,-\infty)(1-\sigma|\mu|^2|E|^2\sin^2\theta_0)\\
&= A_{XZX}\chi^{(2)}_{g,XZX}(-\infty) - A_{XZX}N_g(-\infty)\alpha^{(2)}_{g,zzz}\int d\theta_t\sin\theta_t\int d\theta_0\sin\theta_0(\cos\theta_t - c_{XZX}\cos^3\theta_t)G(\theta_t,t;\theta_0,0)\rho_g(\theta,-\infty)\sigma|\mu|^2|E|^2\sin^2\theta_0\\
&= \chi^{(2)}_{g,XZX}(-\infty) - A_{XZX}N_g(-\infty)\sigma|\mu|^2|E|^2\alpha^{(2)}_{g,zzz}\int d\theta_t\sin\theta_t\int d\theta_0\sin\theta_0(\cos\theta_t - c_{XZX}\cos^3\theta_t)G(\theta_t,t;\theta_0,0)\rho_g(\theta,-\infty)\sin^2\theta_0\\
&= \chi^{(2)}_{g,XZX}(-\infty) - A_{XZX}N_g(-\infty)\sigma|\mu|^2|E|^2\alpha^{(2)}_{g,zzz}(\langle\cos\theta(t)\rangle - c_{XZX}\langle\cos^3\theta(t)\rangle),
\end{aligned} \tag{8}$$

Published under license by AIP Publishing

where

$$\langle \cos\theta(t)\rangle = \int d\theta_t \sin\theta_t \int d\theta_0 \sin\theta_0 \cos\theta_t G(\theta_t, t;\theta_0, 0)\rho_g(\theta, -\infty)\sin^2\theta_0,$$
$$\langle \cos^3\theta(t)\rangle = \int d\theta_t \sin\theta_t \int d\theta_0 \sin\theta_0 \cos^3\theta_t G(\theta_t, t;\theta_0, 0)\rho_g(\theta, -\infty)\sin^2\theta_0. \quad (9)$$

The concrete formula for A_{xzx} and C_{xzx} as well as A and C for other polarization combinations is found in the previous work.[27,48,51–53] In this work, the resultant SFG wavelengths for the −C=O and $-CF_3$ group of coumarin 153 fall at ca. 375 nm and 380 nm, respectively. The fundamental light of 400 nm picosecond light and the SFG lights are close to the maximum absorption peak of coumarin 153 of interest. As such, the ground state SFG experiments here are considered as near doubly resonant SFG.[54]

Likewise, the time evolution of the orientational population for the non-equilibrium excited state is given by $G(\theta_t,t;\theta_0,0)\rho_g(\theta,-\infty)$ $N_g(-\infty)\sigma|\mu|^2|E|^2\sin^2\theta_0$. Thus, the time-dependent susceptibility for the excited state is expressed as

$$\begin{aligned}\chi^{(2)}_{e,XZX}(t) &= A_{XZX}\alpha^{(2)}_{e,zzz}\int d\theta_t \sin\theta_t \int d\theta_0 \sin\theta_0(\cos\theta_t - c_{XZX}\cos^3\theta_t)N_e(\theta, t>0)\\ &= A_{XZX}\alpha^{(2)}_{e,zzz}\int d\theta_t \sin\theta_t \int d\theta_0 \sin\theta_0(\cos\theta_t - c_{XZX}\cos^3\theta_t)G(\theta_t, t;\theta_0, 0)\rho_g(\theta, -\infty)N_g(-\infty)\sigma|\mu|^2|E|^2\sin^2\theta_0\\ &= A_{XZX}N_g(-\infty)\sigma|\mu|^2|E|^2\alpha^{(2)}_{e,zzz}\int d\theta_t \sin\theta_t \int d\theta_0 \sin\theta_0(\cos\theta_t - c_{XZX}\cos^3\theta_t)G(\theta_t, t;\theta_0, 0)\rho_g(\theta, -\infty)\sin^2\theta_0\\ &= A_{XZX}N_g(-\infty)\sigma|\mu|^2|E|^2\alpha^{(2)}_{e,zzz}(\langle\cos\theta_t\rangle - c_{XZX}\langle\cos^3\theta_t\rangle). \end{aligned} \quad (10)$$

After excitation, the total susceptibility is[30,32]

$$\chi^{(2)}_{total,XZX}(t) = \chi^{(2)}_{g,XZX}(t) + \chi^{(2)}_{e,XZX}(t). \quad (11)$$

Although both the ground state and the excited state could contribute to the time-dependent responses, the transient signal from the ground state dominates upon photoexcitation. For transient absorption spectroscopy (or pump-probe) in bulk, ground state bleaching (GSB) and ground state recovery (GSR), excited state absorption (ESA) and stimulated emission (SE) are expected to be observed after photoexcitation. GSB/GSR and SE show negative spectral features in transient absorption spectra, whereas ESA exhibits positive response in the absorption. For the transient SFG experiments, we anticipated to observe the similar behaviors of the photoexcited molecules at interfaces to those in bulk. In particular, a red shift in SFG spectra of excited states is anticipated upon photoexcitation. However, we did not find any spectral shift but only decrease in SFG signals at different time delays upon photoexcitation of coumarin 153 at the air/water interface. There were some possibilities that we could not observe any spectral shift in the excited state of coumarin 153. First of all, the hyperpolarizabilities for the −C=O and $-CF_3$ groups in coumarin 153 for excited states might be too weak to be observed under our experimental conditions. Although our experimental detection limit was on the order of 1% for the change in SFG signal, it might not be sensitive enough to detect weak signals from the excited states. Second, a spectral shift in excited states for the two groups could be too small to be seen in our experimental case. Third, signal-to-noise ratio improvements in collection and sampling methods, or laser systems, are required in the future to observe spectral shifts in excited states. Based on our experimental observations and those above-mentioned possibilities, we suggested that the time-dependent SFG signal is primarily from the recovery of the functional groups of coumarin 153 in the ground state.

Thus, the transient SFG intensity of the *SPS* polarization combination with a circularly polarized pump pulse propagating along the normal to the surface can be expressed by the following:

$$\begin{aligned} I^{XZX}_{SFG}(t) &\propto \left|\chi^{(2)}_{g,XZX}(-\infty) - A_{XZX}N_g(-\infty)\sigma|\mu|^2|E|^2\alpha^{(2)}_{g,zzz}\left[(\langle\cos\theta(t)\rangle - c_{XZX}\langle\cos^3\theta(t)\rangle)\right]\right|^2\\ &\approx I^{XZX}_{SFG}(-\infty) - 2A_{XZX}\chi^{(2)}_{g,XZX}(-\infty)\alpha^{(2)}_{g,zzz}N_g(-\infty)\sigma|\mu|^2|E|^2\alpha^{(2)}_{g,zzz}(\langle\cos\theta(t)\rangle - c_{XZX}\langle\cos^3\theta(t)\rangle). \end{aligned} \quad (12)$$

The change of time-dependent SFG with respect to that at equilibrium is given by the following expression for the SSP intensity measurements:

Published under license by AIP Publishing

$$\frac{\Delta I^{(2)}_{SSP}(t)}{I^{(2)}_{SSP}(-\infty)} = \frac{I^{(2)}_{SSP}(t) - I^{(2)}_{SSP}(-\infty)}{I^{(2)}_{SSP}(-\infty)} \approx -\frac{2\sigma|\mu|^2|E|^2}{N_g(-\infty)} \frac{\langle\cos\theta(t)\rangle - c_{XXZ}\langle\cos^3\theta(t)\rangle}{\langle\cos\theta(-\infty)\rangle - c_{XXZ}\langle\cos^3\theta(-\infty)\rangle}. \quad (13)$$

Experimentally, the quantities of interest are the changes in the intensities of *SSP* and *SPS* at different delay times *t*, namely, $\frac{\Delta I^{(2)}_{SSP}(t)}{I^{(2)}_{SSP}(-\infty)}$ and $\frac{\Delta I^{(2)}_{SPS}(t)}{I^{(2)}_{SPS}(-\infty)}$. By dividing the *SSP* and *SPS* terms by their value at t = 0, one obtains the following:

$$\frac{\frac{\Delta I^{(2)}_{SSP}(t=0)}{I^{(2)}_{SSP}(-\infty)}}{\frac{\Delta I^{(2)}_{SPS}(t=0)}{I^{(2)}_{SPS}(-\infty)}} = \frac{\frac{\langle\cos\theta(t=0)\rangle - c_{XXZ}\langle\cos^3\theta(t=0)\rangle}{\langle\cos\theta(-\infty)\rangle - c_{XXZ}\langle\cos^3\theta(-\infty)\rangle}}{\frac{\langle\cos\theta(t=0)\rangle - c_{XZX}\langle\cos^3\theta(t=0)\rangle}{\langle\cos\theta(-\infty)\rangle - c_{XZX}\langle\cos^3\theta(-\infty)\rangle}} = \frac{\frac{\langle\cos\theta(-\infty)\rangle - \langle\cos^3\theta(-\infty)\rangle - c_{XXZ}(\langle\cos^3\theta(-\infty)\rangle - \langle\cos^5\theta(-\infty)\rangle)}{\langle\cos\theta(-\infty)\rangle - c_{XXZ}\langle\cos^3\theta(-\infty)\rangle}}{\frac{\langle\cos\theta(-\infty)\rangle - \langle\cos^3\theta(-\infty)\rangle - c_{XZX}(\langle\cos^3\theta(-\infty)\rangle - \langle\cos^5\theta(-\infty)\rangle)}{\langle\cos\theta(-\infty)\rangle - c_{XZX}\langle\cos^3\theta(-\infty)\rangle}}. \quad (14)$$

Knowing $D(-\infty)$ and the left hand side term in Eq. (14) enables us to extract $\frac{\langle\cos^3\theta(-\infty)\rangle}{\langle\cos^5\theta(-\infty)\rangle}$ as reported in our earlier work.[17,42,48] If we assume the model that molecules at interfaces wobble in a cone, then a tilt angle and half-angle of the cone can be calculated as documented in previous work. On calculation of the tilt angle and the half-angle, the following terms $\langle\cos\theta(t=0)\rangle$, $\langle\cos^3\theta(t=0)\rangle$, $\langle\cos\theta(-\infty)\rangle$, and $\langle\cos^3\theta(-\infty)\rangle$ can be extracted and thereby the pre-factor $\frac{2\sigma|\mu|^2|E|^2}{N_g(-\infty)}$ in Eq. (13) can be obtained.

Knowing the pre-factor, $\langle\cos\theta(-\infty)\rangle$ and $\langle\cos^3\theta(-\infty)\rangle$, the two time-correlation functions $\langle\cos\theta(t)\rangle$ and $\langle\cos^3\theta(t)\rangle$ were obtained. Thus, we are able to write time-dependent order parameter $D(t)$,

$$D(t) = \frac{\langle\cos\theta(t)\rangle}{\langle\cos^3\theta(t)\rangle}. \quad (15)$$

From $\langle\cos\theta(t)\rangle$ and $\langle\cos^3\theta(t)\rangle$, we obtain the time-dependent average orientational angle $\langle\theta\rangle$ at each time delay. From this, the rate of interfacial orientational motions for molecules at interfaces is obtained.

III. EXPERIMENTAL SECTION

The experimental details of the visible pump-vibrational SFG probe measurements have been introduced in previous papers.[31,32] Briefly, an 800 nm regeneratively amplified Ti:sapphire system (Spitfire, Spectra Physics) seeded with a MaiTai 80 MHz, 80 fs oscillator, at 1 kHz repetition frequency was employed in the present experiments. A reflected 20% output from the regenerative amplifier was used to produce a picosecond 400 nm pulse.[31,32] With difference frequency generation in a 1 mm $AgGaS_2$ crystal, tunable infrared lights between 3 μm and 8.5 μm with a bandwidth of about 150 cm^{-1} (FWHM) were generated from 45% of the output power. The remaining 35% of the 800 nm femtosecond pulse is introduced into another optical parametric amplifier (OPA) to generate a 1.68 μm idler light. The final femtosecond 409 nm light of 0.5 μJ was produced by fourth harmonic generation of the idler light from the second OPA as a pump. The pump wavelength was chosen to be close to the absorption maximum of C153 in solution cite.[55–57]

The IR beam with a typical power of 1.5 μJ per pulse at 5.7 μm and 0.5 μJ per pulse at 7.7 μm was focused onto the sample by a BaF_2 lens with a 100 mm focal length at an angle of 67° relative to the surface normal with a spot size of around 120 μm. The 400 nm picosecond light was focused to 210 μm spot size by a BaF_2 lens with a 250 mm focal length at an angle of 76° from the surface normal. The 409 nm pump light was focused on the sample from the top by a BaF_2 lens with a 500 mm focal length along the surface normal with a focal spot of 800 μm. The polarization of the circularly polarized pump beam was controlled using a quarter wave plate.

A 300 mm spectrograph with one entry and two exits (Acton Research, three gratings including 1200 grooves/mm with 450 nm blazed, 1200 grooves/mm with 500 nm blazed and 600 grooves/mm with 4 μm blazed) was used. The 450 nm blazed grating was chosen to measure SFG signals. One exit was configured for detecting the dispersed signal with a liquid-nitrogen cooled, back-thinned charged coupled device (CCD) camera (Roper Scientific, 1340 × 400 pixels) operating at −120 °C. The generated SFG signal was focused into the monochromator and detected by a photomultiplier tube (PMT) (Hamamatsu) when the time-profile experiments were performed. The signal from PMT was sent into a BOXCAR averager and then into a lock-in amplifier with reference to a 500 Hz chopper frequency in the pump light arm. Two probe beams were guaranteed to overlap temporally at the maximum SFG signals in all the experiments. A translational stage and the signal sampling from the lock-in amplifier were controlled by a Labview program.

The purity of C153 was checked to be 99.0% by high-performance liquid chromatography (HPLC) and used without further purification. The Gibbs monolayers of C153 were prepared by allowing the C153 solution to stand for 30 minutes prior to the start of laser experimentation in order to allow for complete formation of the monolayers. The Teflon beakers were cleaned prior to use by immersion in freshly prepared piranha solution for 20 min and then rinsed with copious amounts of ultrapure water in order to remove any trace organics. Surface tension measurements were performed with a Wilhelmy plate method. The sample was contained in a shallow Teflon beaker mounted on a stage rotating at 2.5 rpm to minimize heating and degradation effects in SFG experiments. The

Published under license by AIP Publishing

SFG signal level from a probe alone was checked to ensure whether samples were degraded over the time. The typical time for a single forward and backward scan was 10 min. After three cycles, it was found that the probe SFG signal had not changed. We found that after five cycles (about 50 min), the signal level decreased by 10%. To ensure no photo-degradation of samples, a fresh sample was always made after 30 min; namely, three cycles of forward and backward scans.

IV. RESULTS AND DISCUSSION

A. Surface excess of C153 at the air/water interface

To obtain information on the population of C153 at the air/water interface, we used Gibb's adsorption equation, which is given by[1,2]

$$\Gamma = -\frac{1}{RT}\frac{\partial \gamma}{\partial \ln c}, \tag{16}$$

where Γ is the surface excess of C153, c is the C153 concentration in solution, and γ is the surface tension. The surface tension as a function of C153 concentration is shown in Fig. 2. The surface excess at bulk concentration c is obtained by taking a derivative of the surface tension at each concentration, which thereby yields the moles of C153 per unit area. The concentration of a typical SFG experiment was 8 μm, which corresponds to a surface area of around 660 Å^2.

B. SFG measurements of C153 at the air/water interface

Figure 3(a) shows the SFG spectra of an 8 μm C153 aqueous solution taken at the four different polarization combinations *SSP*, *PPP*, *SPS*, and *PSS* with the visible beam at 400 nm and the IR centered at 1700 cm^{-1} with a bandwidth of 150 cm^{-1}. There is only one peak observed at 1718 cm^{-1} in all the polarization spectra. This peak was assigned to the stretching mode of the —C=O group of C153. It was found that the SFG intensities differ for the different polarization combinations. The SFG signals of the *SSP* polarization are almost three times stronger than those of the *PPP* polarization. The intensities of the *SPS* and *PSS* polarization are almost identical, being nearly ten times weaker than those of the *SSP* polarization. These ratios are used to find the orientation angle of the —C=O group of C153.

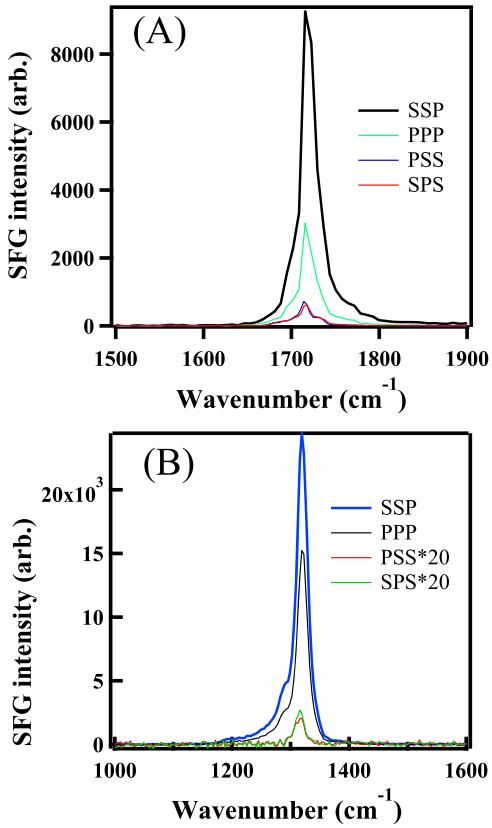

FIG. 3. (a) The SFG spectra of 8 μm C153 for four different polarization combinations (*SSP*, *PPP*, *SPS*, and *PSS*). In (a), the peak at 1718 cm^{-1} is assigned to the stretching mode of the —C=O group of C153. In (b), the peak at 1319 cm^{-1} is assigned to the stretching mode of the —CF_3 group of C153.

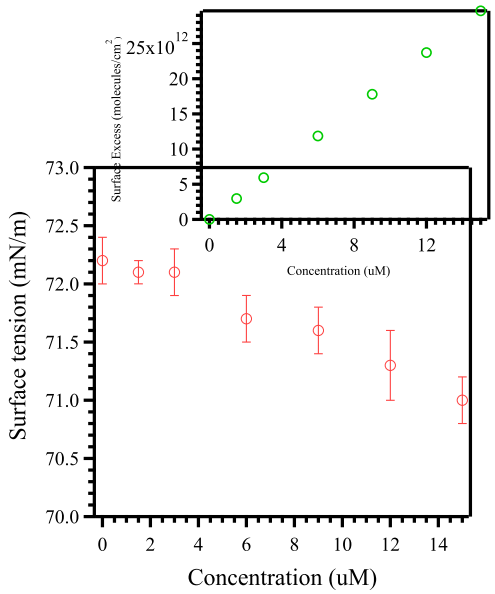

FIG. 2. Surface tension vs. C153 concentration in aqueous solution. The surface excess calculated is shown in the inset.

Figure 3(b) shows the SFG spectra of 8 μm C153 aqueous solution taken at the four different polarization combinations *SSP*, *PPP*, *SPS*, and *PSS* with the visible beam at 400 nm and the IR centered at 1300 cm^{-1} with a bandwidth of 150 cm^{-1}. The main peak at 1319 cm^{-1} appears in the four polarization spectra. We assigned the peak to the symmetric stretching mode of —CF_3 in the ring of C153.[58] The SFG intensity for the *SSP* polarization is slightly stronger than that of the *PPP* polarization. The SFG intensities for the *SPS* and *PSS* polarization are almost identical, being nearly 100 times weaker than those of the *SSP* polarization. These ratios are used to find the orientation angle of the —CF_3 group of C153.

Published under license by AIP Publishing

C. Absolute orientational structure of C153 at the air/water interface

The approach that we employed to determine absolute orientational structure was established in earlier work.[42] Briefly measurements of the intensity ratio between the different polarization combinations yielded the interfacial orientational order parameter $D(-\infty)$ prior to the pump pulse, as shown in Eq. (7). From the order parameter $D(-\infty)$, the average orientational angles of the $-C=O$ group and $-CF_3$ groups of C153 with respect to the surface normal were extracted. Based on the relative orientation of the two groups in the C153 molecule and the SFG measured orientations of the two groups, the absolute orientation of the C153 molecule can be found.

Using the intensity ratios between the different polarization combinations shown in Figs. 3(a) and 3(b) and using Eq. (7), we found the orientational angles of the $-C=O$ and $-CF_3$ groups to be 144° and 59° with respect to the surface normal assuming a narrow orientational distribution. Combining these two measurements with the known angle of 120° between the $-C=O$ and $-CF_3$ symmetric stretch axes, we obtained the absolute orientation of the C153 molecules at the air/water interface. The angle of the normal to the molecular plane with respect to the interface normal was found to be 55°, which is also the angle between the molecular plane and the surface plane. In Fig. 4, the orientational structure of C153 at the air/water interface is shown.

D. Orientational dynamics of the individual $-C=O$ and $-CF_3$ groups

Figure 5(a) shows the time traces for SFG intensities of the $-C=O$ group in the C153 molecule for both the *SSP* and *SPS* polarization combinations, respectively. This figure plots the ratio of the normalized SFG intensities to the SFG intensities at $t < 0$ ($I(t)/I(-\infty)$) versus the time delay of the pump pulse (with respect to the probe pulses). The solid lines of these traces were fitted to a single exponential that gives a recovery time of 105 ± 11 ps for the *SSP* combination and a recovery time of 62 ± 5 ps for the *SPS* combination. These recovery times differ for the two polarization combinations because of the different sensitivity to the pump-induced non-equilibrium orientational distribution for each polarization combination. The time-dependent responses for different polarization combinations are a result of different weighted sums of $\langle\cos\theta(t)\rangle$ and $\langle\cos^3\theta(t)\rangle$, as shown in Eq. (13). These recovery times were attributed to out-of-plane orientational relaxation time of the $-C=O$ group of C153 at the air/water interface.

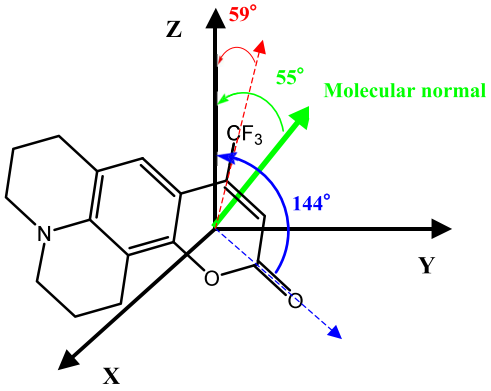

FIG. 4. An absolute orientational configuration of C153 at the air/water interface. The orientational angles for the $-C=O$, $-CF_3$, and the molecular normal are 144°, 59°, and 55°, respectively.

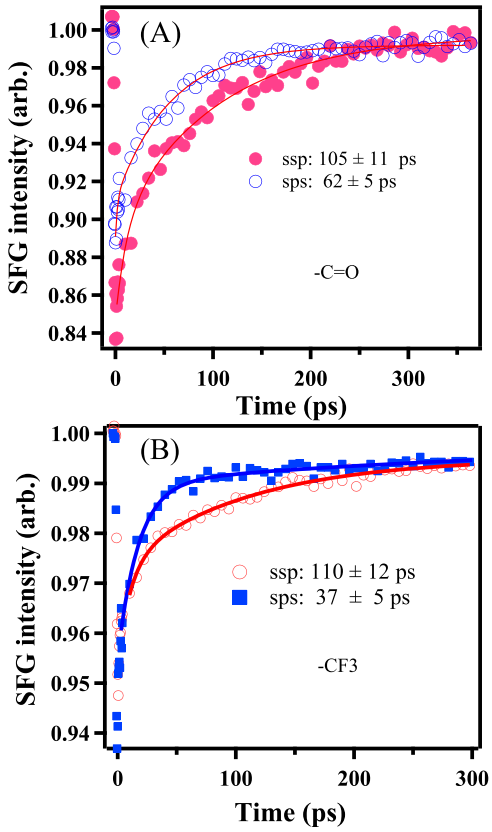

FIG. 5. The time traces of SFG intensities of *SSP* and *SPS* for the $-C=O$ group (a) and the $-CF_3$ group (b) with respect to the SFG intensities at $t < 0$ after photo-excitation of a circularly polarized pump incident along the surface normal.

Figure 5(b) displays the time traces for the SFG intensities of the $-CF_3$ group in the C153 molecule for both the *SSP* and *SPS* polarization combinations. Using the methods employed for Fig. 5(a), we found that the recovery time of *SSP* is 110 ± 12 ps and the recovery time of the *SPS* is considerably faster being 37 ± 5 ps.

E. Absolute orientational dynamics

Figures 6(a) and 6(b) show the time-dependence of the orientational angles of the $-C=O$ and $-CF_3$ groups in the C153 molecule. Upon excitation at t = 0, the vibrational $-C=O$ dipole moment rotates from 148° back to the measured ground state equilibrium orientational angle of 144° (the $-C=O$ angle before photoexcitation). The time constant for this orientational relaxation was found to be 130 ± 20 ps. The $-CF_3$ group exhibited a rotation from 65° back to our measured ground state equilibrium orientation angle of 59° with a time constant of 210 ± 38 ps. Once these time-dependent

Published under license by AIP Publishing

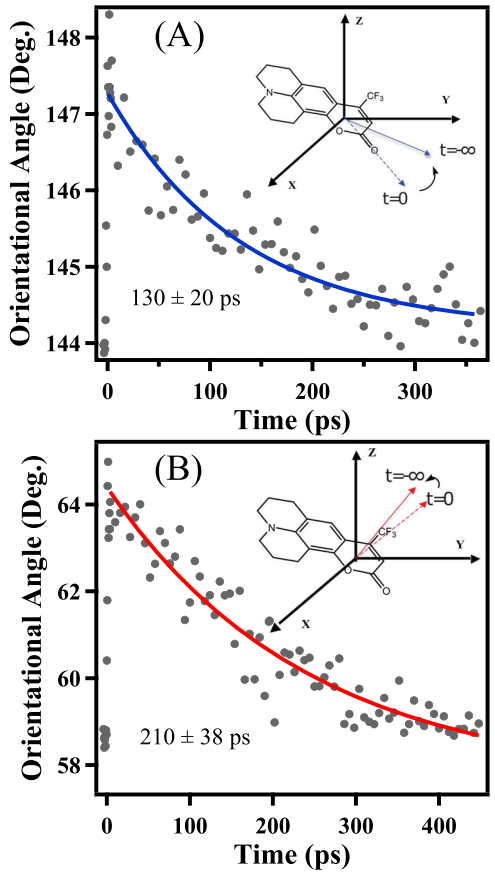

FIG. 6. The time-dependent average orientational angle for the —C=O group shown in (a) and the —CF_3 group shown in (b).

orientational angles of —C=O are known, the orientational motions of the normal to the molecular plane of C153 with respect to the surface normal were found. The angle of the normal to the molecular plane with respect to the interface normal as a function of time is shown in Fig. 7. When excited, the normal to the molecular plane rotates from its pump induced non-equilibrium value of 58° to its ground state equilibrium value of 55°, with a time constant of 125 ± 26 ps.

F. Interfacial orientational diffusion

For orientational relaxation in bulk liquids, the evolution function can be obtained from an orientational diffusion model. Due to the complexity of rotational motions in the anisotropic environment of an interface, we do not, at this time, have a model for molecular motions in an interfacial region. However, the wobbling-in-a-cone model has had some success in describing the orientational dynamics in restricted environments.[41,42,59–64] The basic idea for the wobbling-in-a-cone model is that the motion of the probe molecule is described as diffusive ("wobbling") within a cone of a certain semi-angle and diffusion outside the cone is forbidden. Within the framework of this model, an analytical expression of the diffusion coefficient for wobbling that relates the relaxation time to the semi-angle

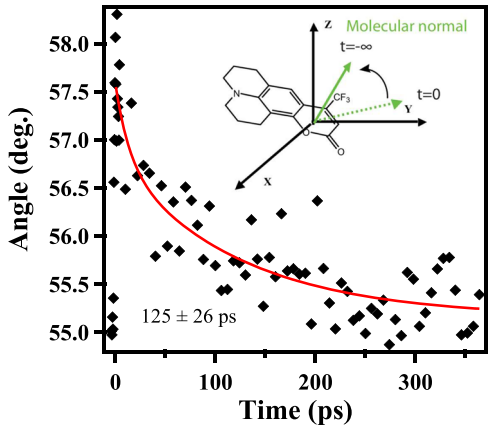

FIG. 7. The time-dependent average orientational angle for the molecular normal to the molecular plane of C153.

of the cone. Although this model is simple, it has been successfully applied to rotational diffusion of lipids and proteins in a lipid matrix. Based on the model, the interfacial orientational diffusion coefficient D_θ is expressed as $D_\theta = \frac{1}{2}\lim_{t\to\infty}\frac{\langle[\theta_t-\theta_{t=0}]\rangle^2}{t} = \frac{1}{2}\frac{\langle\Delta\theta^2\rangle}{\tau}$, where $\Delta\theta$ is the maximum change in the orientational angle upon photo-excitation and τ is a measured orientational relaxation time. On application of this model, we found that the interfacial orientational diffusion coefficients for the —C=O and —CF_3 groups are 9.4×10^{-6} ps^{-1} and 2.2×10^{-5} ps^{-1}, which are two orders of magnitude slower than rotational diffusion of C153 in bulk water.[59,65] It is important to note that the changes in the orientational angles for —C=O and —CF_3 have been obtained for a delta orientational distribution. The orientational distribution for —C=O and —CF_3 groups was found to be 4.5° and 6.8°, respectively. Previous SHG studies also showed that Coumarin 314 (C314) at the air/water interface has a narrow orientational distribution width of 16°, which corresponds to a half angle of 8° for the case of wobbling diffusion. These results indicate that C153 and C314 molecules are well ordered at the interface through interactions with interfacial water solvents. Although the cone model used above is an oversimplification of the real potential energy of interfacial molecules in the interfacial environment, our findings suggest that at the air/water interface C153 molecules experience a much stronger out-of-plane friction than the friction in bulk water.

A molecular dynamics calculation found that orientational motions in the interfacial region depend strongly on the polarity and location of the adsorbates.[66] Molecular dynamics simulations of C314 at the air/water interface yielded a number of equilibrium and dynamics properties.[67] The calculated orientation of C314 is in good agreement with experimental results. Calculations of the ground and excited state dipole moments were also found to be in reasonable agreement with the measured values. However, simulations of dynamic processes for C314 at the air/aqueous interface are more difficult to carry out. The out-of-plane rotational correlation relaxation times obtained from simulations were roughly an order of magnitude faster than the experimental results found in the work reported here. This discrepancy can be attributed to the simulation correlation time expression that involves the $\langle\cos\theta(t)\cos\theta(0)\rangle$

Published under license by AIP Publishing

time correlation function, whereas the SHG and SFG time correlation functions involve terms such as $\langle \cos^3\theta(t)\cos^2\theta(0)\rangle$ as well as $\langle \cos\theta(t)\cos^2\theta(0)\rangle$.[67] It would be of value to carry out a simulation for the rotational correlation function using terms such as $\langle \cos^3\theta(t)\cos^2\theta(0)\rangle$ and $\langle \cos\theta(t)\cos^2\theta(0)\rangle$, which describe the temporal correlation function obtained from SHG and SFG measurements. Even though a new simulation would be useful, the orientation calculated from our simplified model still can give the orientation of C153 at the interface in three dimensions. The technique we used can help study interfacial interactions as well as study molecular motions during chemical reactions that occur at an interface.

V. CONCLUSIONS

We have measured the absolute 3 dimensional rotational motions of Coumarin 153 (C153) at an air/water interface using the time-resolved polarized Sum Frequency Generation (TR-SFG) technique. To begin with the equilibrium orientations of the symmetry axes of the −C=O, the CF_3 groups with respect to the interface normal were measured when C153 was in its ground electronic state. By perturbing the equilibrium orientational distribution of C153, we then measured the time dependence of the absolute orientations of the two chromophores as the C153 molecules rotate toward their equilibrium orientations. Perturbation of the equilibrium orientational distribution was achieved by photoexciting a subset of the equilibrium distribution with a polarized pump pulse that is resonant with the lowest excited singlet state of C153. The polarization of the pump pulse determines the contribution of in-plane and out-of-plane rotations to the measured SFG intensity. Using a circularly polarized pump pulse that was incident normal to the interface enabled us to separate the out of-plane from the in-plane rotations. The photoselection process using the circularly polarized pump pulse shifted the average orientation of the C=O group by an increase of $4^\circ \pm 0.6^\circ$. The rotational recovery time was found to be 130 ± 20 ps, which is the time to reach the equilibrium orientational distribution. The orientational change in the normal to the molecular plane was found to be $4^\circ \pm 0.5^\circ$ with a rotational recovery time of 125 ± 26 ps. It is also noted that, as given above, the transient shift in orientation and the orientational relaxation dynamics of the −C=O group and the angle of the normal to the molecular plane with respect to the normal of the interfacial plane are the same. We believe that these observations act as guidance in understanding bond-making and bond-breaking in photochemistry, in particular, spatial selectivity of chemical reactions at interfaces and surfaces.

SUPPLEMENTARY MATERIAL

See supplementary material for time-dependent SFG responses under SSP and PPP for the –C=O group and the $-CF_3$ group of coumarin 153 at the air/water interface.

ACKNOWLEDGMENTS

K.B.E. is thankful for generous support of this research through Award No. CHE-1360969. Y.R. is thankful for generous support of this research through Award No. CHE-1506789. The authors also thank Dr. Michael Fayer, Dr. Tony F. Heinz, and Dr. Dezheng Sun for their helpful discussions.

The authors declare no competing financial interest

REFERENCES

[1] P. B. Miranda and Y. R. Shen, J. Phys. Chem. B **103**, 3292 (1999).
[2] Y. R. Shen, Annu. Rev. Phys. Chem. **40**, 327 (1989).
[3] Y. R. Shen, *The Principles of Nonlinear Optics* (John Wiley & Sons, Inc., Hoboken, New Jersey, 2003).
[4] K. B. Eisenthal, Chem. Rev. **96**, 1343 (1996).
[5] F. M. Geiger, Annu. Rev. Phys. Chem. **60**, 61 (2009).
[6] A. L. Mifflin, M. J. Musorrafiti, C. T. Konek, and F. M. Geiger, J. Phys. Chem. B **109**, 24386 (2005).
[7] O. Esenturk and R. A. Walker, J. Chem. Phys. **125**, 174701 (2006).
[8] J. T. Fourkas, R. A. Walker, S. Z. Can, and E. Gershgoren, J. Phys. Chem. C **111**, 8902 (2007).
[9] Y. B. Fan, X. Chen, L. J. Yang, P. S. Cremer, and Y. Q. Gao, J. Phys. Chem. B **113**, 11672 (2009).
[10] S. Kataoka and P. S. Cremer, J. Am. Chem. Soc. **128**, 5516 (2006).
[11] X. Y. Chen, H. Z. Tang, M. A. Even, J. Wang, G. N. Tew, and Z. Chen, J. Am. Chem. Soc. **128**, 2711 (2006).
[12] J. C. Conboy and M. A. Kriech, Anal. Chim. Acta **496**, 143 (2003).
[13] M. J. Shultz, S. Baldelli, C. Schnitzer, and D. Simonelli, J. Phys. Chem. B **106**, 5313 (2002).
[14] S. Baldelli, Acc. Chem. Res. **41**, 421 (2008).
[15] M. Xu, R. Spinney, and H. C. Allen, J. Phys. Chem. B **113**, 4102 (2009).
[16] W. Gan, D. Wu, Z. Zhang, R. R. Feng, and H. F. Wang, J. Chem. Phys. **124**, 114705 (2006).
[17] H. F. Wang, W. Gan, R. Lu, Y. Rao, and B. H. Wu, Int. Rev. Phys. Chem. **24**, 191 (2005).
[18] J. A. Carter, Z. H. Wang, and D. D. Dlott, Acc. Chem. Res. **42**, 1343 (2009).
[19] Z. H. Wang, D. G. Cahill, J. A. Carter, Y. K. Koh, A. Lagutchev, N. H. Seong, and D. D. Dlott, Chem. Phys. **350**, 31 (2008).
[20] M. Sovago, E. Vartiainen, and M. Bonn, J. Chem. Phys. **131**, 161107 (2009).
[21] G. J. Simpson, J. M. Perry, and C. L. Ashmore-Good, Phys. Rev. B **66**, 165437 (2002).
[22] L. Fu, J. Liu, and E. C. Y. Yan, J. Am. Chem. Soc. **133**, 8094 (2011).
[23] A. D. Curtis, M. C. Asplund, and J. E. Patterson, J. Phys. Chem. C **115**, 19303 (2011).
[24] J. E. Laaser, W. Xiong, and M. T. Zanni, J. Phys. Chem. B **115**, 2536 (2011).
[25] A. V. Benderskii, J. Henzie, S. Basu, X. M. Shang, and K. B. Eisenthal, J. Phys. Chem. B **108**, 14017 (2004).
[26] K. T. Nguyen, X. M. Shang, and K. B. Eisenthal, J. Phys. Chem. B **110**, 19788 (2006).
[27] Y. Rao, S. Y. Hong, N. J. Turro, and K. B. Eisenthal, J. Phys. Chem. C **115**, 11678 (2011).
[28] X. M. Shang, K. Nguyen, Y. Rao, and K. B. Eisenthal, J. Phys. Chem. C **112**, 20375 (2008).
[29] X. Shi, E. Borguet, A. N. Tarnovsky, and K. B. Eisenthal, Chem. Phys. **205**, 167 (1996).
[30] D. Zimdars, J. I. Dadap, K. B. Eisenthal, and T. F. Heinz, J. Phys. Chem. B **103**, 3425 (1999).
[31] Y. Rao, N. J. Turro, and K. B. Eisenthal, J. Phys. Chem. C **114**, 17703 (2010).
[32] Y. Rao, D. H. Song, N. J. Turro, and K. B. Eisenthal, J. Phys. Chem. B **112**, 13572 (2008).
[33] J. A. McGuire and Y. R. Shen, Science **313**, 1945 (2006).
[34] P. Sen, S. Yamaguchi, and T. Tahara, Faraday Discuss. **145**, 411 (2010).
[35] C.-S. Hsieh, R. K. Campen, A. C. Vila Verde, P. Bolhuis, H.-K. Nienhuys, and M. Bonn, Phys. Rev. Lett. **107**, 116102 (2011).
[36] Z. Zhang, L. Piatkowski, H. J. Bakker, and M. Bonn, Nat. Chem **3**, 888 (2011).
[37] A. Eftekhari-Bafrooei and E. Borguet, J. Am. Chem. Soc. **132**, 3756 (2010).
[38] K. B. Eisenthal, Acc. Chem. Res. **26**, 636 (1993).

Published under license by AIP Publishing

[39]T. Araiso and T. Koyama, Chem. Phys. Lipids **50**, 105 (1989).
[40]A. Castro, E. V. Sitzmann, D. Zhang, and K. B. Eisenthal, J. Phys. Chem. **95**, 6752 (1991).
[41]M. P. Heitz and F. V. Bright, Appl. Spectrosc. **49**, 20 (1995).
[42]Y. Rao, M. Comstock, and K. B. Eisenthal, J. Phys. Chem. B **110**, 1727 (2006).
[43]X. Wei, S. C. Hong, X. W. Zhuang, T. Goto, and Y. R. Shen, Phys. Rev. E **62**, 5160 (2000).
[44]C. Hirose, N. Akamatsu, and K. Domen, Appl. Spectrosc. **46**, 1051 (1992).
[45]C. Hirose, N. Akamatsu, and K. Domen, J. Chem. Phys. **96**, 997 (1992).
[46]D. Zhang, J. Gutow, and K. B. Eisenthal, J. Phys. Chem. **98**, 13729 (1994).
[47]X. Zhuang, P. B. Miranda, D. Kim, and Y. R. Shen, Phys. Rev. B **59**, 12632 (1999).
[48]Y. Rao, Y. S. Tao, and H. F. Wang, J. Chem. Phys. **119**, 5226 (2003).
[49]D. Zimdars and K. B. Eisenthal, J. Phys. Chem. B **105**, 3993 (2001).
[50]A. V. Benderskii and K. B. Eisenthal, J. Phys. Chem. B **104**, 11723 (2000).
[51]R. Lu, W. Gan, B.-h. Wu, H. Chen, and H.-f. Wang, J. Phys. Chem. C **108**, 7297 (2004).
[52]R. Lu, W. Gan, B.-h. Wu, Z. Zhang, Y. Guo, and H.-F. Wang, J. Phys. Chem. B **109**, 14118 (2004).
[53]Y. Rao, M. Xu, S. Jockusch, N. J. Turro, and K. B. Eisenthal, Chem. Phys. Lett. **544**, 1 (2012).
[54]M. B. Raschke, M. Hayashi, S. H. Lin, and Y. R. Shen, Chem. Phys. Lett. **359**, 367 (2002).
[55]Y. Jiang, P. K. McCarthy, and G. J. Blanchard, Chem. Phys. **183**, 249 (1994).
[56]R. Improta, V. Barone, and F. Santoro, Angew. Chem., Int. Ed. **46**, 405 (2007).
[57]S. A. Kovalenko, J. Ruthmann, and N. P. Ernsting, Chem. Phys. Lett. **271**, 40 (1997).
[58]C. B. Kristalyn, S. Watt, S. A. Spanninga, R. A. Barnard, K. Nguyen, and Z. Chen, J. Colloid Interface Sci. **353**, 322 (2011).
[59]Z. Gengeliczki, D. E. Rosenfeld, and M. D. Fayer, J. Chem. Phys. **132**, 244703 (2010).
[60]P. B. Moore, C. F. Lopez, and M. L. Klein, Biophys. J. **81**, 2484 (2001).
[61]J. P. Starck, Y. Nakatani, G. Ourisson, D. J. Cowley, and G. Duportail, New J. Chem. **20**, 1293 (1996).
[62]M. Tarek, D. J. Tobias, and M. L. Klein, J. Phys. Chem. **99**, 1393 (1995).
[63]H. Saito, T. Araiso, H. Shirahama, and T. Koyama, J. Biochem. **109**, 559 (1991).
[64]N. Kimura, R. Tsuneta, T. Araiso, T. Koyama, N. Hasegawa, T. Ishii, and K. Mukasa, Chem. Phys. Lipids **57**, 39 (1991).
[65]C. C. Wang and R. Pecora, J. Chem. Phys. **72**, 5333 (1980).
[66]M. L. Johnson, C. Rodriguez, and I. Benjamin, J. Phys. Chem. A **113**, 2086 (2009).
[67]D. A. Pantano and D. Laria, J. Phys. Chem. B **107**, 2971 (2003).

Published under license by AIP Publishing